

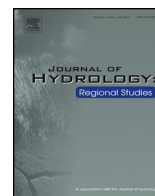


ELSEVIER

Contents lists available at ScienceDirect

# Journal of Hydrology: Regional Studies

journal homepage: [www.elsevier.com/locate/ejrh](http://www.elsevier.com/locate/ejrh)



## Interpretation of gravity data to delineate underground structure in the Beppu geothermal field, central Kyushu, Japan

Jun Nishijima<sup>a,\*</sup>, Kento Naritomi<sup>b</sup>

<sup>a</sup> Department of Earth Resources Engineering, Faculty of Engineering, Kyushu University, 744 Motoooka Nishi-ku, Fukuoka 819-0395, Japan

<sup>b</sup> Department of Earth Resources Engineering, Graduate School of Engineering, Kyushu University, Japan

### ARTICLE INFO

#### Article history:

Received 17 July 2015

Received in revised form

21 November 2015

Accepted 30 November 2015

Available online xxx

#### Keywords:

Gravity

Beppu geothermal field

Hot spring

Hydrothermal system

### ABSTRACT

*Study region:* The area of the Beppu geothermal field is located in southeast Japan (33° 15' to 20' N, 131° 27' to 32' E).

*Study focus:* The Beppu geothermal field, which is one of the largest hot-spring resorts, is located in the eastern end of the Beppu-Shimabara Graben, in central Kyushu, Japan. Details of the subsurface structure are necessary for hydrothermal modeling and numerical simulation. This study aims to delineate the shallow underground fault and basement structure using gravity analysis.

*New hydrological insights for the region:* A high Bouguer anomaly is detected in the southern part of this area, which corresponds to the distribution of the Kankaiji andesite. The results of the edge-detection filter of gravity data indicate that the northern edge of the high Bouguer anomaly corresponds to the Asamigawa Fault in the southern part of the study area, but deviates 1 km southeast of the Kankaiji hot spring to the north. In this area of high value, which indicates the fault, three hot spring areas, Horita, Kankaiji and Hamawaki, are located. The distribution of the depths of the three-dimensional gravity basement enables the delineation of the interface between the volcanic basement rocks and the fan deposit. The conspicuous, steep slope of the gravity basement is detected along the Asamigawa Fault and the southern hot-spring area. However, the northern hot-spring area is distributed on the uplift of the gravity basement. The results of the gravity analysis indicate that the structure of the hot-spring water path differs between the southern and northern hot-spring areas.

© 2015 The Authors. Published by Elsevier B.V. This is an open access article under the CC BY license (<http://creativecommons.org/licenses/by/4.0/>).

## 1. Introduction

Beppu is one of the largest hot-spring resorts in southwestern Japan and includes several hot-spring areas (Fig. 1). Thermal activities such as hot springs and fumaroles can be seen in many places in this area. These thermal activities are developed on the eastern flanks of Mt. Tsurumi and Mt. Garandake, which are located at the eastern end of the Beppu-Shimabara Graben. Based on previous research, it is inferred that the hydrothermal activity is maintained by up-flow of the parent geothermal fluid, which has a temperature of 250–300 °C, beneath the cones of Mt. Tsurumidake and Mt. Garandake. This parent fluid

\* Corresponding author.

E-mail address: [nishijima@mine.kyushu-u.ac.jp](mailto:nishijima@mine.kyushu-u.ac.jp) (J. Nishijima).

<http://dx.doi.org/10.1016/j.ejrh.2015.11.022>

2214-5818/© 2015 The Authors. Published by Elsevier B.V. This is an open access article under the CC BY license (<http://creativecommons.org/licenses/by/4.0/>).

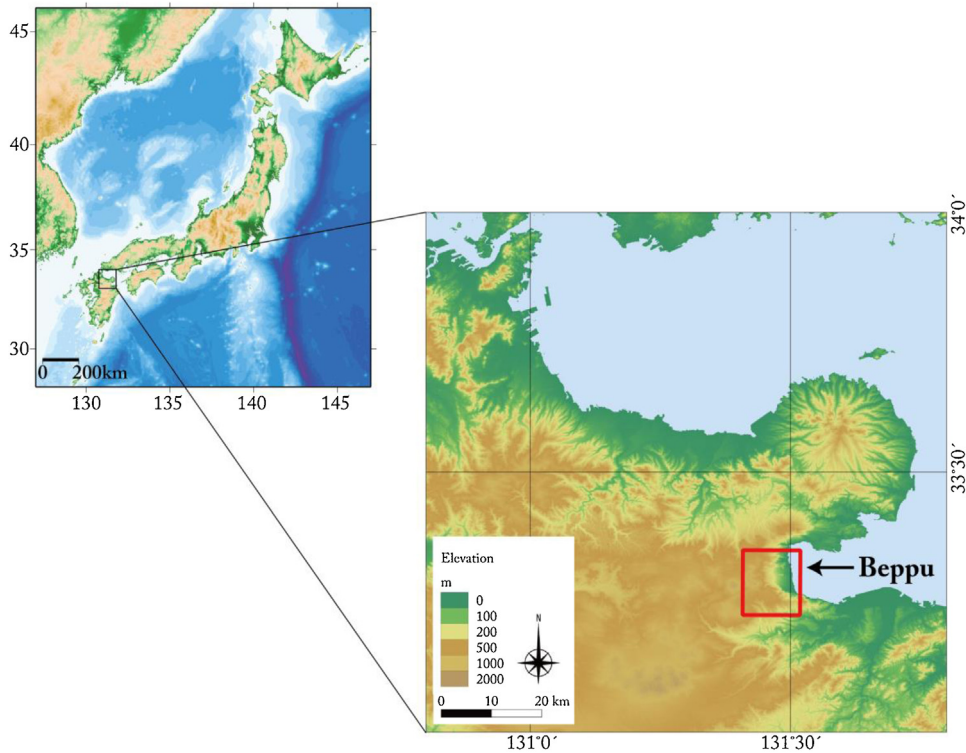
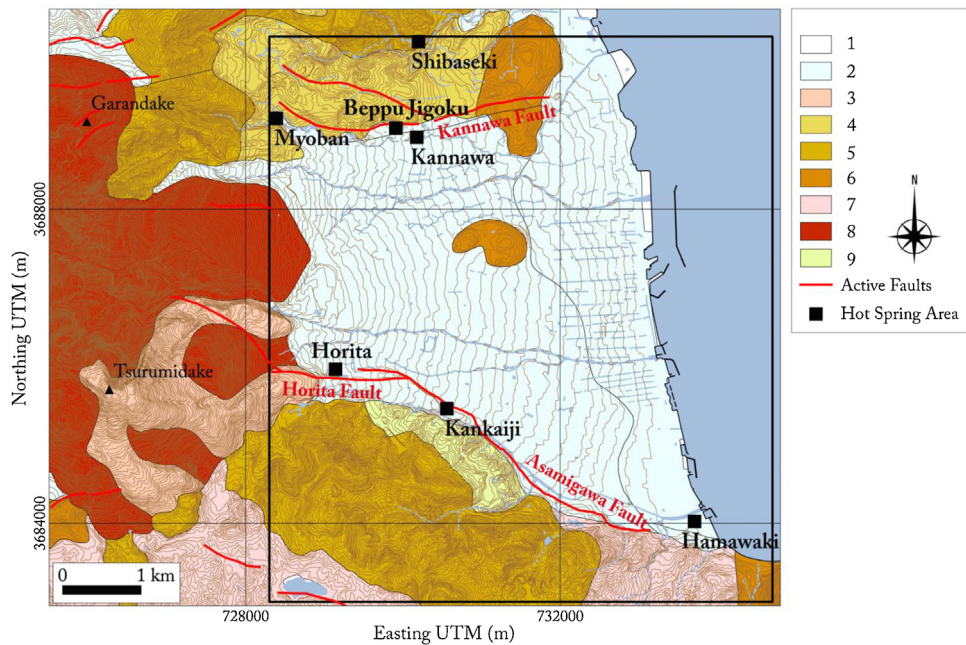
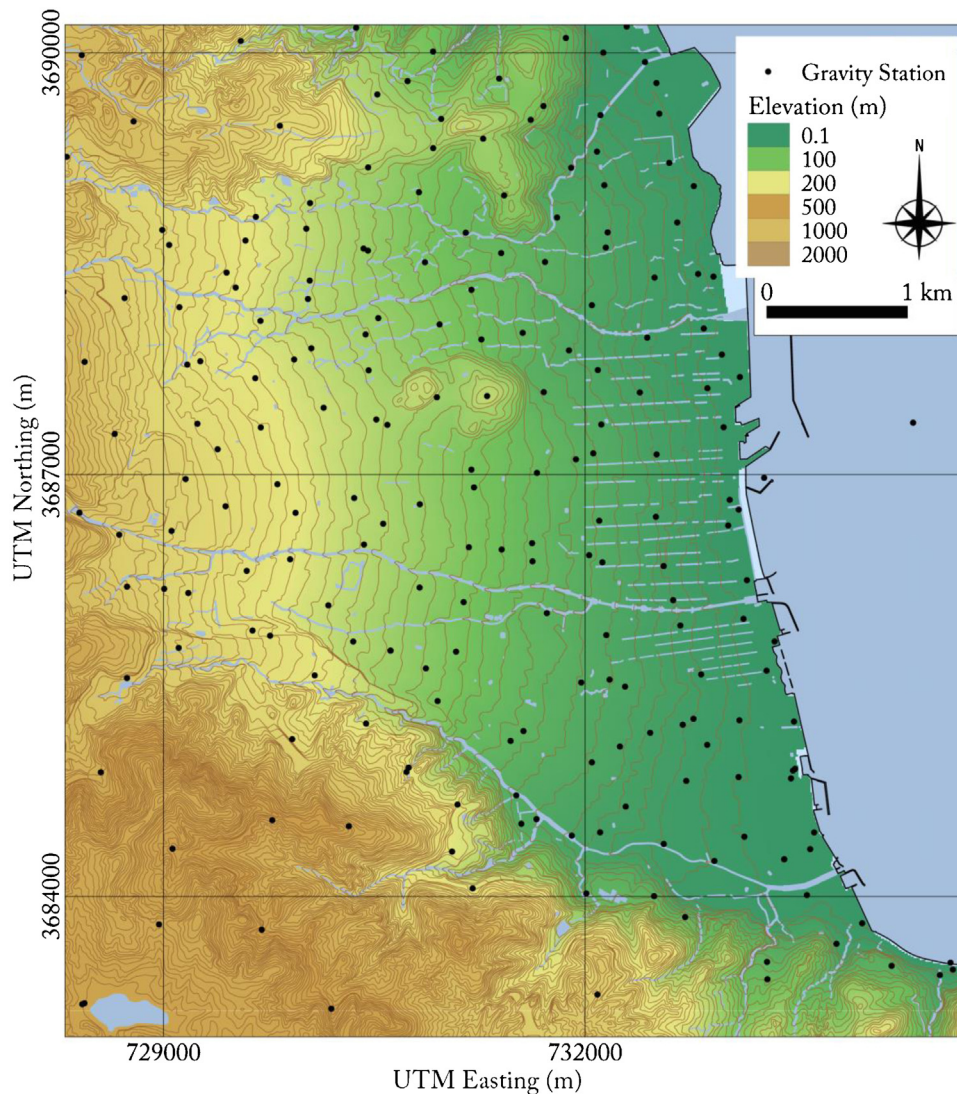


Fig. 1. Location of the Beppu geothermal field, central Kyushu, Japan.



1: Reclaimed Land 2: Fan Deposit 3: Trurumi Summit Andesite 4: Matsuzuka Debris Avalanche Deposit 5: Takahirayama Lava 6: Jissoujiyama Dacite 7: Yufugawa Pyrocrastic Flow Deposit 8: Garandake Andesite 9: Kankaiji Andesite

Fig. 2. Geological map of the study area and its surroundings, modified from the Geological Survey of Japan (2014). The red line and the black square show the location of the active faults (Chida et al., 2000) and hot-spring area, respectively. The black rectangle shows the study area.



**Fig. 3.** Topography of the study area. The black line and dots show the location of the active faults (Chida et al., 2000) and the gravity stations in Figs. 3–10.

flows to the coast along the two major flow paths, which form the southern and the northern hot-spring areas (Allis and Yusa, 1989).

Exploitation of the Beppu hydrothermal system began as early as the 1880s, and the amount of production from the hot springs is increasing (Yusa et al., 2000). It is important to assess the sustainability of the hot springs for long-term use. The detailed investigation of subsurface structure is necessary for hydrothermal modeling and assessment of numerical simulation. There are various geophysical methods for delineating the underground basement and fault structure. A gravity survey is effective for detecting a fault structure related to a hot-water path (Abdelzaher et al., 2011; Represas et al., 2013). Kusumoto et al. (1996) modeled the density structure in the eastern part of the Beppu-Shimabara Graben, including Beppu city. However, a detailed basement and fault structure of the Beppu geothermal field has not been conducted. Therefore, the aim of this study is to delineate the basement structure of the Beppu geothermal field and to determine its relationship with the hydrothermal systems by applying three-dimensional (3-D) gravity modeling to the available gravity data.

## 2. Geological setting

Beppu Bay is a typical, tectonic-controlled, sedimentary basin, which is called the Beppu-Shimabara Graben and is under the influence of the Philippine Sea convergence plate (Ittoh et al., 2014). According to the distribution of the horizontal crustal strain over 90 years (Tada, 1984), central Kyushu is a tectonically remarkable area where extension tectonics from north to south (N-S) dominate. Therefore, the geological faults in this area are normal faults with east–west (E–W) and northwest–southeast (NW–SE) trending. The Hohi volcanic zone, which is located in the eastern part of the Beppu-Shimabara Graben,

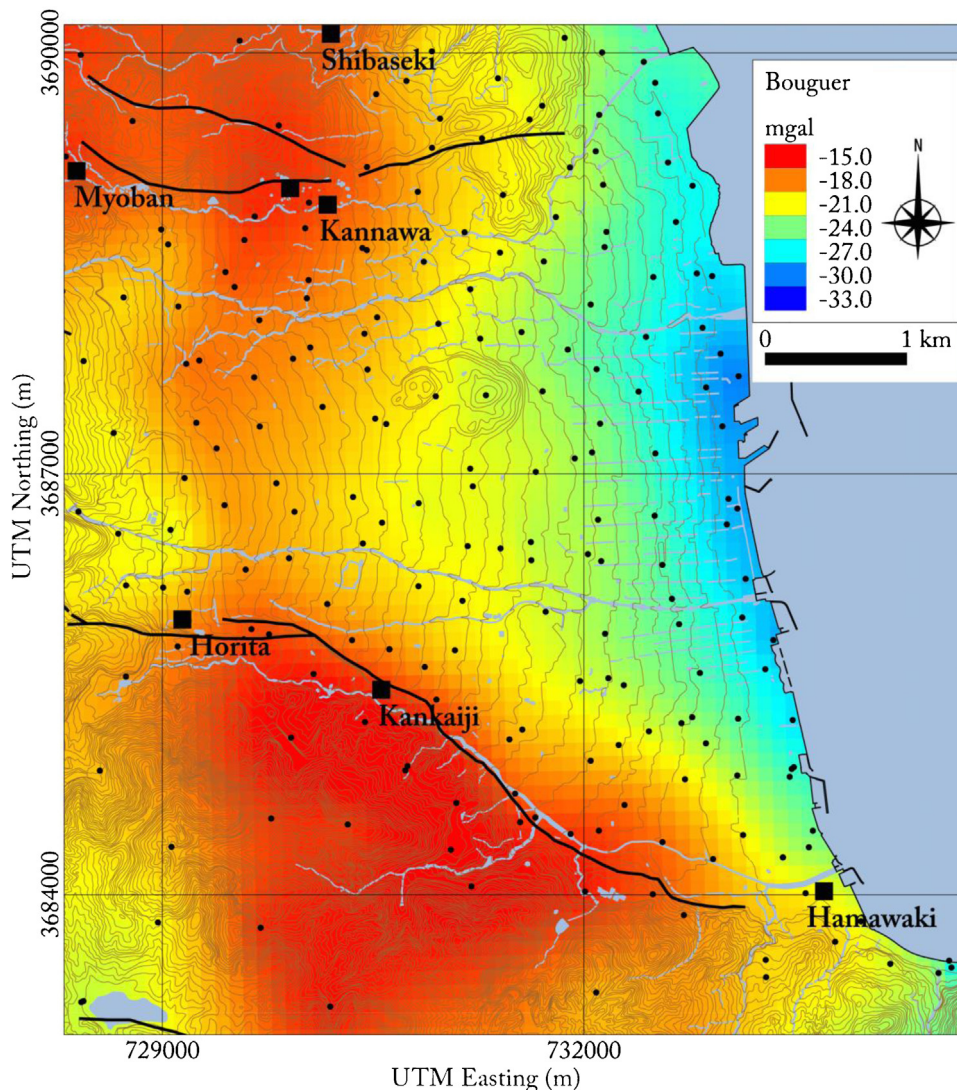


Fig. 4. Bouguer anomalies with an assumed density of  $2350 \text{ kg/m}^3$ . The black dots show the location of the gravity station.

was dominated by volcanic activity during the Neogene and Quaternary (Kamata, 1989). The Beppu geothermal field is located on the eastern flanks of Mt. Tsurumidake and Mt. Garandake, which were late-Quaternary volcanic centers.

Fig. 2 shows a geological map of Beppu city (Geological Survey of Japan, 2014). The geological setting in Beppu comprises Pliocene andesite (Kankaiji and esite), Pleistocene volcanic rocks, and fan sedimentary deposits (Hoshizumi et al., 1988). Cretaceous granite is exposed to the north and south, just outside of the study area (Sasada, 1987). In addition, Cretaceous granite crops out locally in this area. Sasada (1984) pointed out that Cretaceous granite is widespread under northern central Kyushu. Based on gravity analysis, Kusumoto et al. (1996) estimated that the depth of this Cretaceous granite is 2–3 km.

### 3. Gravity data

#### 3.1. Gravity reduction

To make a complete Bouguer anomaly map, this study processed gravity data comprising 206 stations (Geological Survey of Japan, 2013) and covering an area of approximately  $46 \text{ km}^2$  with spacing between 250 m and 2 km (Fig. 3). To complete the Bouguer anomaly, the gravity data was reduced, applying the necessary corrections, such as free-air, Bouguer, and terrain conditions. For the Bouguer and terrain corrections, an assumed density of  $2350 \text{ kg/m}^3$  was determined by an objective Bayesian approach (Murata, 1993). Terrain corrections were calculated using the 50-m mesh digital elevation map of the Geographical Survey Institute (GSI) of Japan. The complete Bouguer anomaly was interpolated to a 100-m grid using the minimum curvature method (Smith and Wessel, 1990). Fig. 4 depicts the Bouguer anomaly map. The Bouguer anomalies

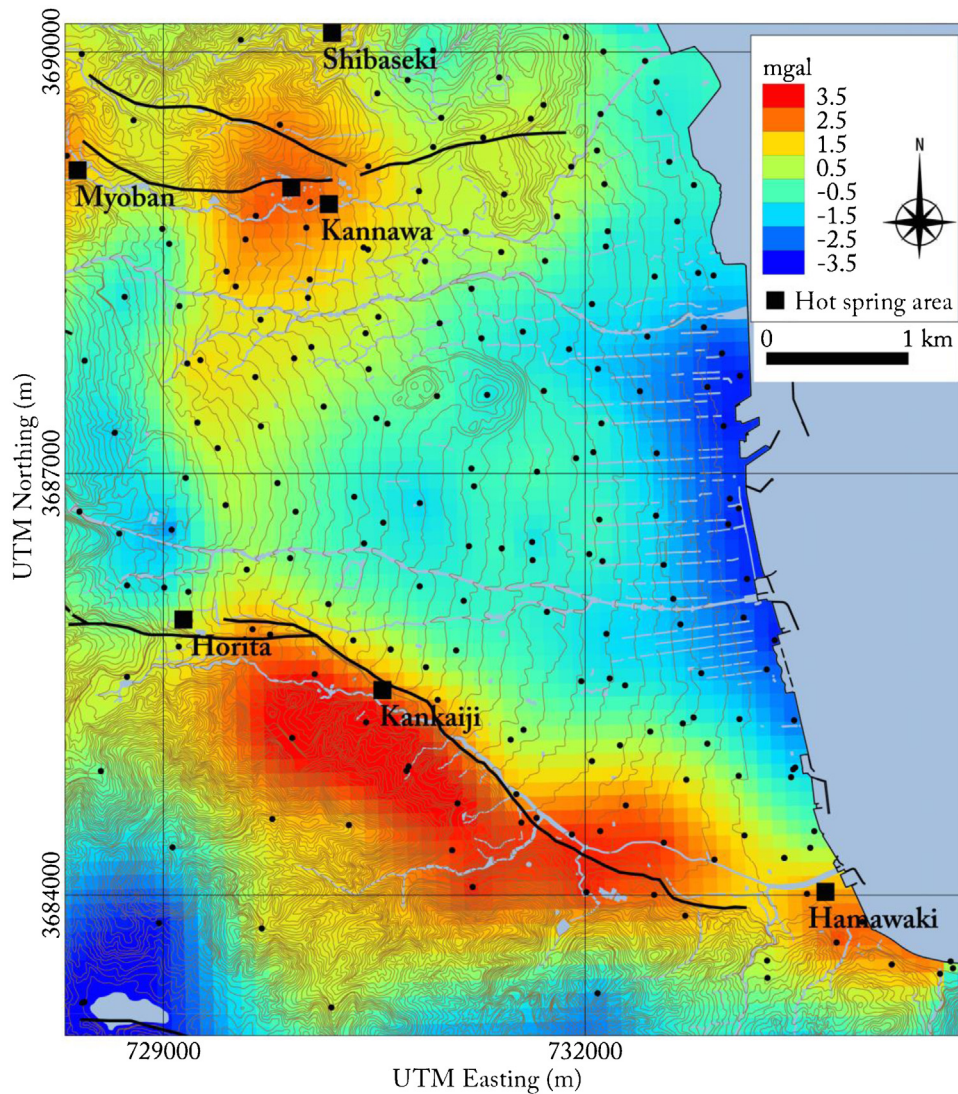


Fig. 5. Residual Bouguer anomaly map. The regional anomaly calculated by second-order polynomial fitting is removed from Fig. 4.

were all negative, ranging from  $-35.5$  m gal to  $-6.5$  m gal, decreasing in the eastern coastal regions of the mapped area. In addition, two high Bouguer anomalies can be seen in the northern and southwestern areas.

### 3.2. Regional-local anomaly separation

The Bouguer anomaly includes the effect of regional trend caused by the deep, large structure. Because this study aims to reveal the shallow gravity basement structure, the regional anomaly was isolated using the second-order polynomial trend (Fig. 5) which is considered to represent the deep, granitic structure.

Fig. 5 shows a high Bouguer anomaly in the southern part of this area. In comparison with Fig. 2, this high anomaly agrees with the distribution of the Kankaiji andesite. In addition, the edge of the high anomaly is consistent with the location of the Horita, Kankaiji, and Hamawaki hot-spring areas. Furthermore, another high anomaly can be seen in the northwestern part of the study area. The Kannawa and Beppu Jigoku areas are located in this high-anomaly area.

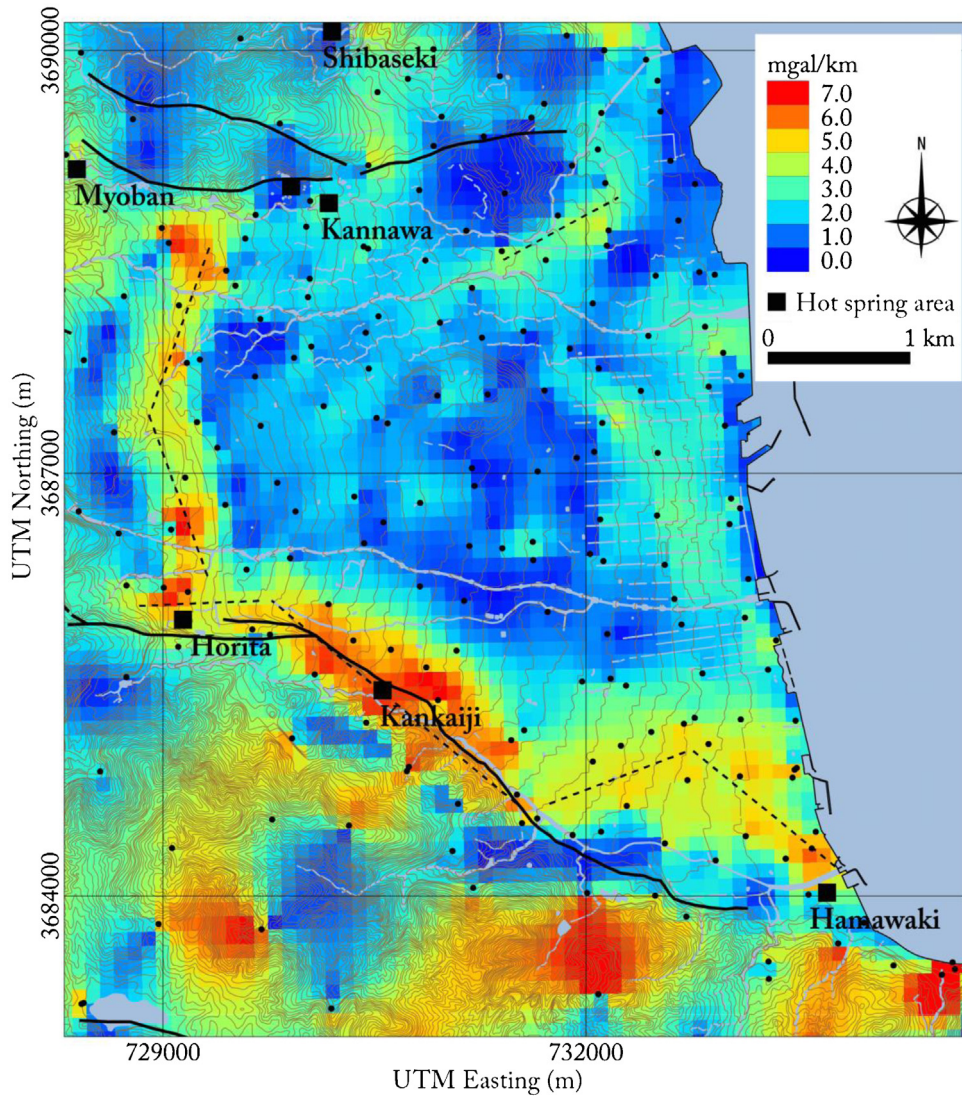


Fig. 6. Horizontal derivatives (HD) of the Bouguer anomaly. The dashed lines show the discontinuities identified using the HD map.

### 3.3. Edge detection filter

There are several methods for detecting the edges caused by fault structures or geological boundaries. Most of these methods are high-pass filters based on the horizontal and vertical derivatives of the gravity anomaly. The horizontal derivative (HD) maximizes above any abrupt change of density (Cordell and Grauch, 1985) and can be given by

$$HD = \sqrt{\left(\frac{\partial g}{\partial x}\right)^2 + \left(\frac{\partial g}{\partial y}\right)^2} \tag{1}$$

where  $(\partial g/\partial x)$  and  $(\partial g/\partial y)$  are the directional derivatives of the gravity anomaly in the  $x$  and  $y$  directions, respectively. Advantages of the HD are less susceptibility to noise and that it can recognize the edges of both shallow and deep structures clearly. Fig. 6 depicts the amplitude of HD in the study area. The dashed line in Fig. 6 corresponds to the Asamigawa Fault in the southern part of the study area, but deviating 1 km southeast of the Kankaiji hot spring to the north. The hot-spring area, which is located in the southern part, near Horita, Kankaiji, and Hamawaki, corresponds to this high HD value. In addition, a high HD with N-S trend was detected on the eastern sides of Mt. Tsurumidake and Mt. Garandake.

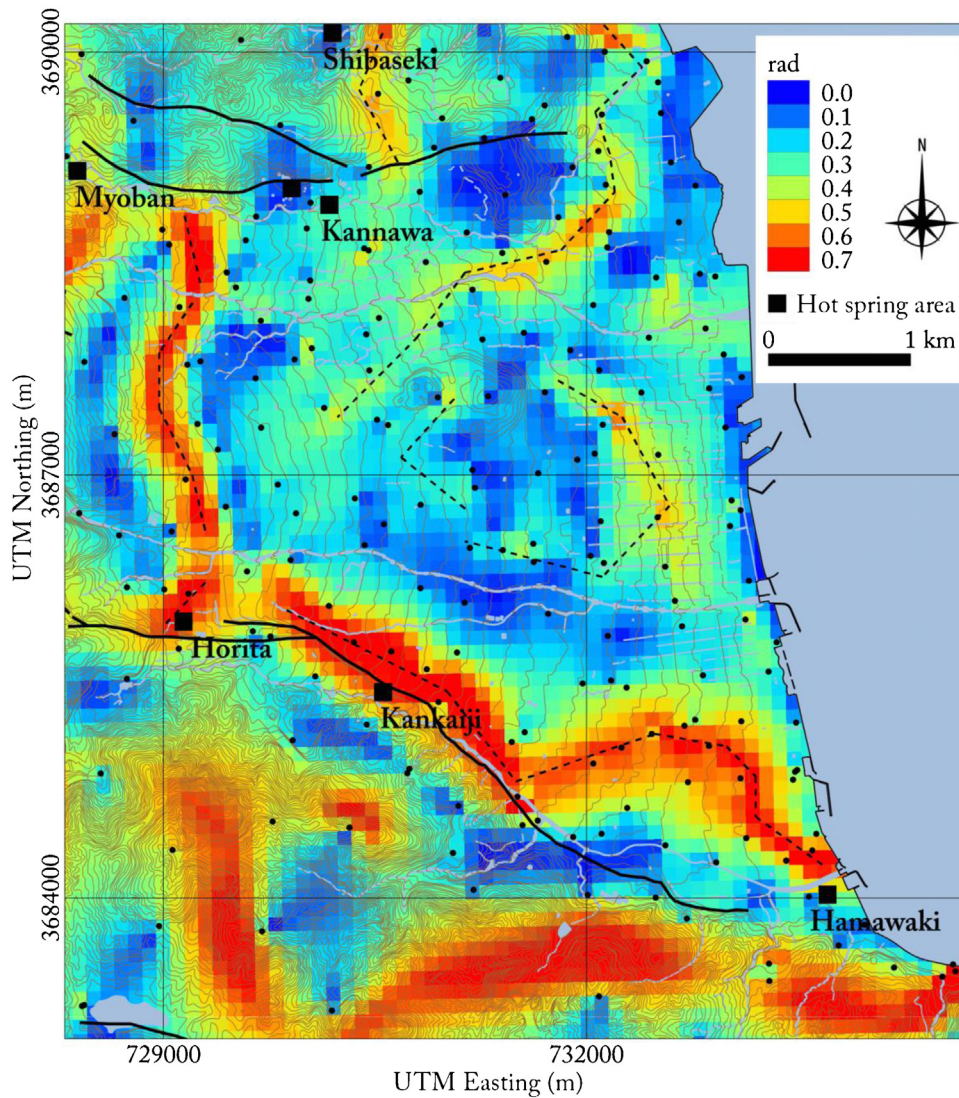


Fig. 7. Improved normalized horizontal tilt angle (INH) map of the Bouguer anomaly. The dashed lines show the discontinuities identified using the INH map.

The improved normalized horizontal tilt angle (INH) filter, proposed by Li et al. (2014), is an edge-detection filter that is an improvement upon the normalized horizontal tilt angle (TDX) filter developed by Cooper and Cowan (2006) and can be given by

$$INH = \tan^{-1} \left( \frac{\sqrt{\left(\frac{\partial g}{\partial x}\right)^2 + \left(\frac{\partial g}{\partial y}\right)^2}}{p + \left|\frac{\partial g}{\partial z}\right|} \right) \quad (2)$$

where  $p$  is a positive constant value and is decided by the interpreter. In general, the value of  $p$  is approximately equal to one-tenth or one-twentieth of the maximum of the total horizontal derivative (Li et al., 2014). Fig. 7 shows the INH of the residual gravity anomaly with  $p$  of 0.005. The value of  $p$  was decided by trial and error. The high INH values in the western and southern parts of the area match well with the HD map (Fig. 6). In addition, a high INH was detected in the eastern part of the Shibaseki hot-spring area and in the nearby coastal area. Although this high INH value was not as clear as that in the southern area, in comparison with the geological map (Fig. 2), this high INH value shows the geological boundary between the Jissoujiyama dacite and the fan deposit. In the southern area, there are some large, anomalous, high-gradient areas caused by a lack of gravity measurement point.

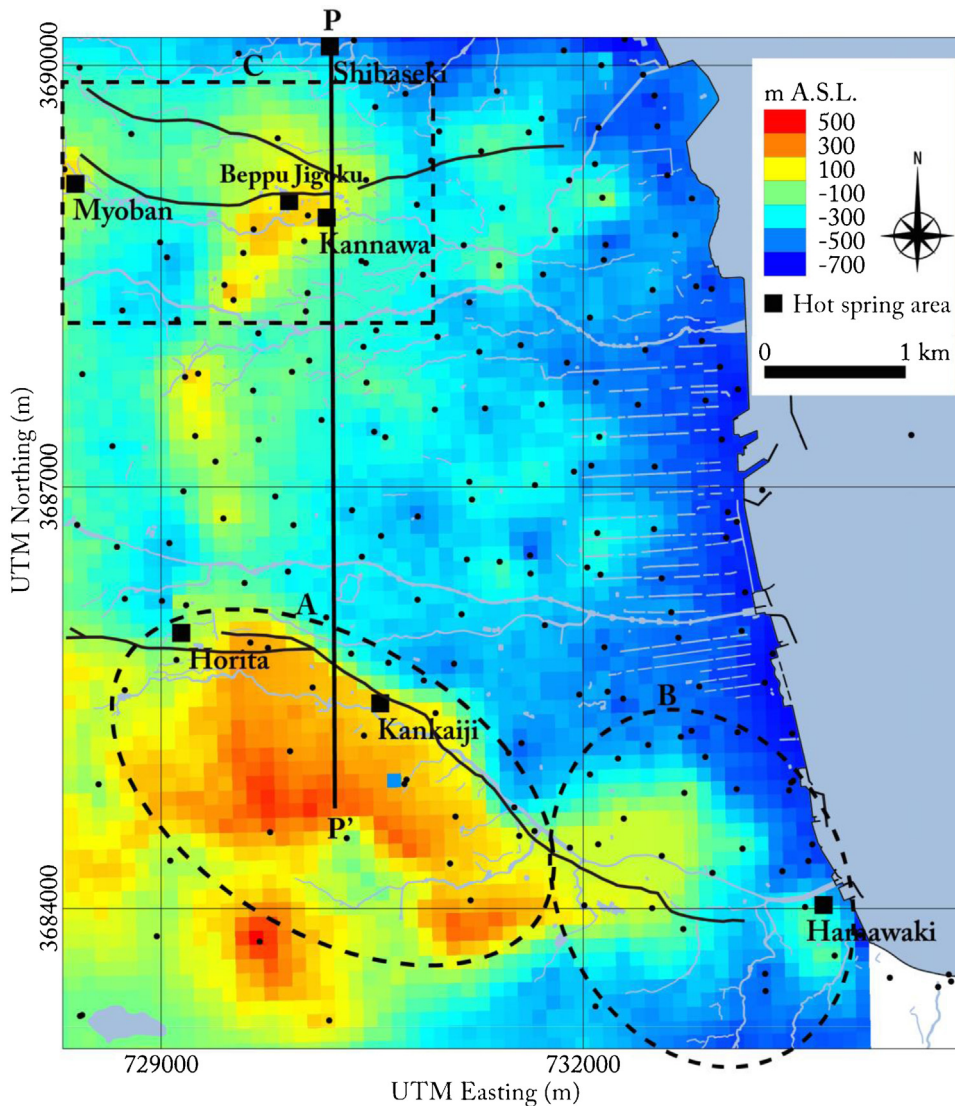


Fig. 8. Gravity basement in meters above sea level with density contrast of  $400 \text{ kg/m}^3$ .

#### 4. Three-dimensional gravity modeling

##### 4.1. Modeling method

The above-mentioned filtering method can easily detect steep gravity gradients that indicate the location of faults or geological boundaries, but it is impossible to estimate their depths. To determine the depth and detailed shape of the volcanic basement rock, 3-D gravity modeling was conducted. Distribution of 3-D gravity basement structures are generally modeled by approximating them to an aggregation of rectangular prisms whose horizontal dimensions are the same as those of the input Bouguer anomaly grid (Cordell and Henderson, 1968; Rao et al., 1999). The gravity anomaly that is caused by each prism can be calculated using an equation (Okabe, 1979) that adjusts the depth of the prisms that form the gravity basement model until it minimize the root mean square error, which is determined by the difference between the measured residual and the calculated Bouguer anomaly.

This modeling method requires a contrast in density. According to the geological map (Hoshizumi et al., 1988) and stratigraphic column (New Energy Development Organization, 1990), it is possible that the survey area can be approximated by two geological layers: the Quaternary fan deposit and the Neogene–Quaternary volcanic basement rock. The thicknesses of the prisms represented the depth from the surface to the basement, and a constant density contrast of  $-400 \text{ kg/m}^3$  was assigned to all prisms. The density of the fan deposit was set at  $1950 \text{ kg/m}^3$ , and the density of the basement rock was set at  $2350 \text{ kg/m}^3$  (New Energy Development Organization, 1990). The horizontal size of the prismatic cells was 100 m.



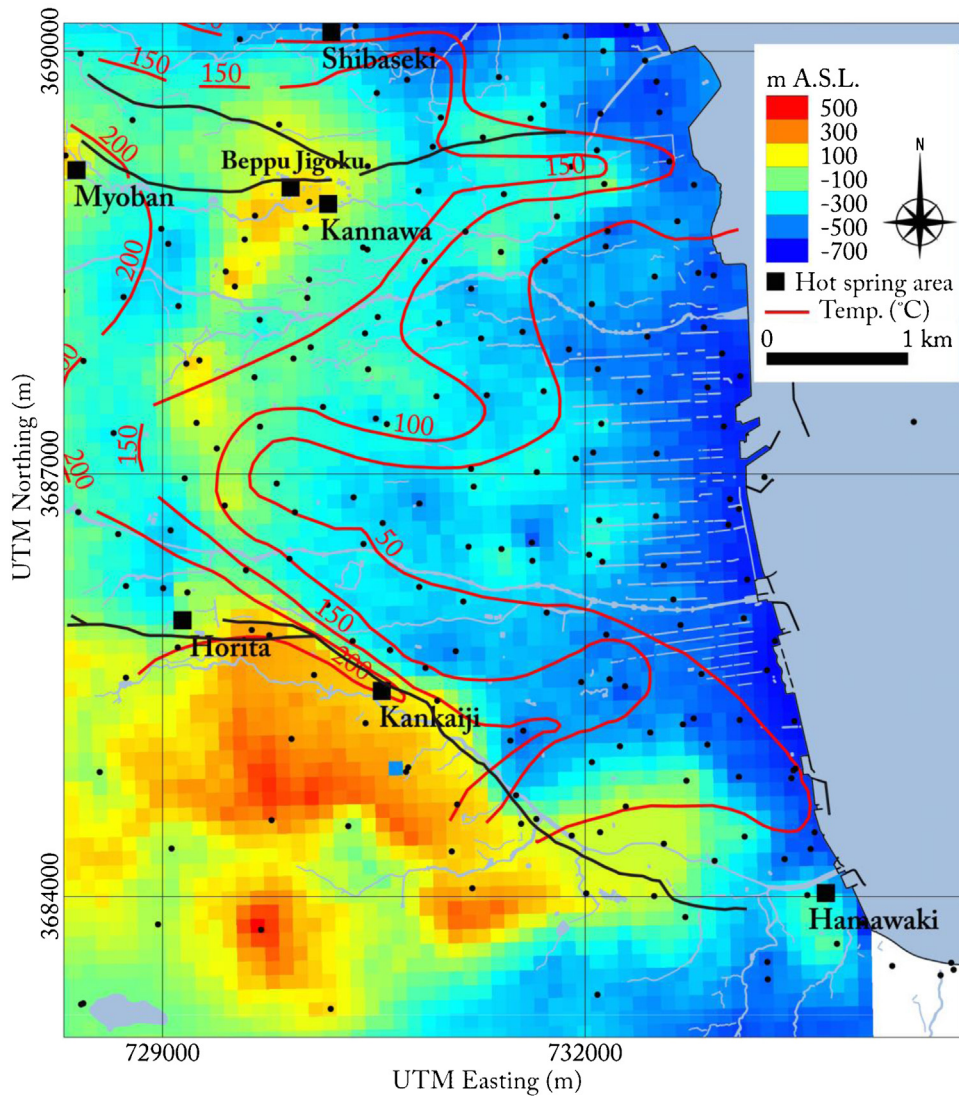


Fig. 9. Comparison between the gravity basement and the isotherm at 100 m below sea level inferred from bottom hole measurements, modified from Allis and Yusa (1989).

#### 4.2. Result of modeling

Fig. 8 shows the results of the 3-D gravity basement analysis. A conspicuous uplift of the gravity basement can be seen in the southern part of the map (A in Fig. 8). The gravity basement is depressed about 700 m along the Asamigawa Fault (A in Fig. 8). The Horita and Kankaiji hot-spring areas are located in the steep depression of the gravity basement. Another uplift of the gravity basement (B in Fig. 8) exists adjacent to the previously mentioned uplift area. The Hamawaki hot-spring area is located at the eastern end of this uplift area. In contrast, the steep depression of the gravity basement cannot be seen in and around the northern hot-spring areas and the Kannawa Fault. The majority of the hot springs are located on the uplift area of the gravity basement (C in Fig. 8).

### 5. Discussion

Allis and Yusa (1989) mapped the temperature at 100 m below sea level and inferred from the bottom hole temperature measurement. This isotherm distribution indicates the existence of two outflow zones of geothermal water that coincide with the northern (Myoban, Kannawa and Beppu Jigoku) and southern (Horita, Kankaiji and Hamawaki) areas of thermal activity (Allis and Yusa, 1989). In comparison with the gravity basement (Fig. 9), the distribution of high temperature (more than 150 °C) corresponds to the Asamigawa Fault. However, these high-temperature areas are located along the southeastern

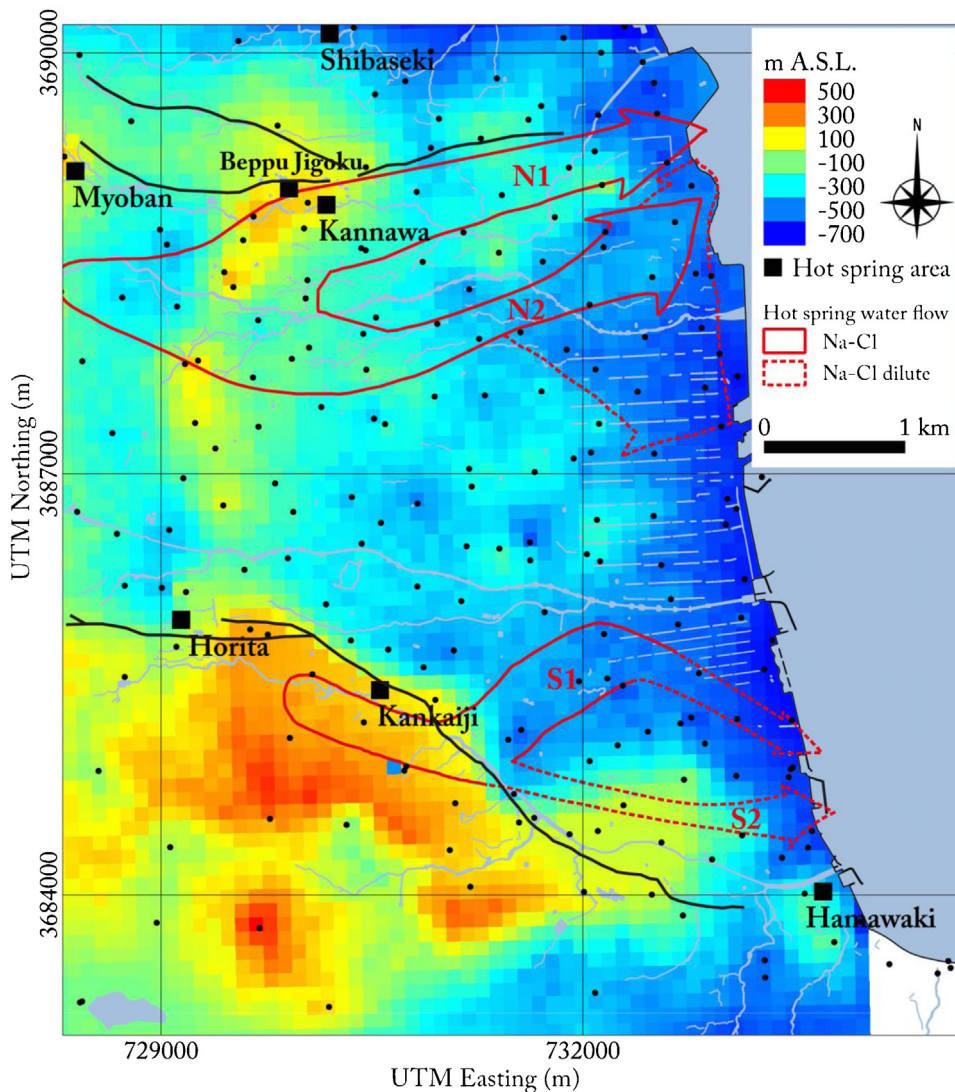


**Fig. 10.** Comparison between the gravity basement and the subsurface flows of the Na-Cl-type hot-spring water inferred from the chemical composition of the hot-spring water, which is modified from Ohsawa et al. (1994) and Osawa (1996).

uplift area (B in Fig. 8). In contrast to the southern part, the high-temperature (more than 150°C) area is widespread in and around the uplift of the gravity basement in the northern area (C in Fig. 8).

Fig. 10 shows the comparison between the gravity basement and the subsurface flow of the Na-Cl-type hot-spring water inferred from chemical composition (Ohsawa et al., 1994; Ohsawa and Yusa, 1996). In the southern part, the hot-spring water's main flow (S1 in Fig. 10) wraps around the northern edge of the gravity basement uplift. Although the reason of this bending of the hot-spring water flow has not been understood by past research, it is clear that the uplift of the gravity basement bends the hot-spring water. In contrast, no remarkable depression, like that of a fault structure, can be seen in the northern hot-spring area, but some part of the hot-spring water flow wraps around the uplift of the gravity basement at the Kannawa hot-spring area.

Fig. 11 shows a cross-section of the P-P' in Fig. 8. A steep gradient of volcanic basement exists below the Shibaseki, Kannawa (A in Fig. 8) and Kankaiji (B in Fig. 8) hot-spring areas. In the Kankaiji hot spring, a steep gradient area corresponds to the Asamigawa Fault, and areas of high hot-spring temperatures are located along this fault. The hot water flows up near the surface through the fault structure. The main flow path of the hot springs is considered to be along the Asamigawa Fault and the southern part of the Kannawa hot-spring area. In contrast, the steep gradient of the volcanic basement could not be found below the Kannawa Fault, although steep gradient areas were found below the Shibaseki and Kannawa hot springs. The northern high-temperature area is widespread above the uplift of the volcanic basement (A in Fig. 8). It is possible that the path of the hot water is not only along the steep gradient area, but also in the small fractures in the basement uplift.

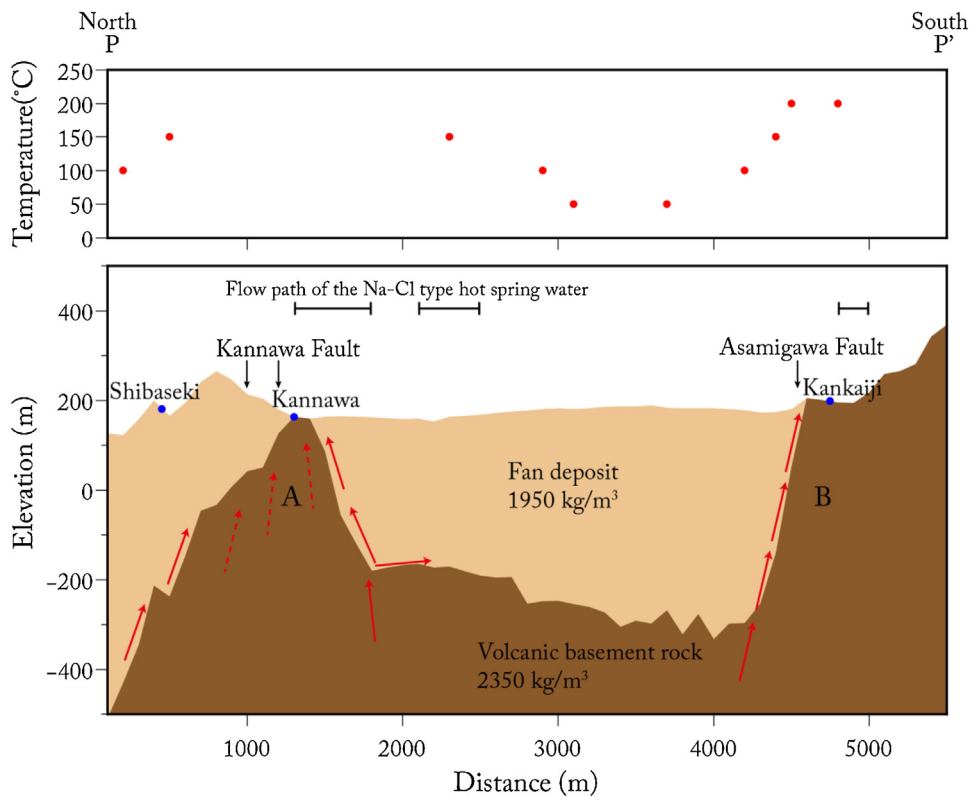


**Fig. 11.** Profile of line P-P' in Fig. 8. The hot-water flows up near the surface through the fault structure. The density of the volcanic basement is assumed to be 2350 kg/m<sup>3</sup> and that of the fan deposit is 1950 kg/m<sup>3</sup>. The main flow path of the hot spring is considered to be a part of the Asamigawa Fault and the southern part of the Kannawa hot-spring area. The graph shows the temperature at 100 m below sea level, which is digitized from Allis and Yusa (1989).

Taking into account the above comparison, it is thought that the structure of the path of the hot-spring water differs between the southern and northern hot-spring areas. In the southern area, the path is controlled by the fault structure along the steep slope of the gravity basement. However, this steep slope cannot be detected in the northern hot-spring area. It is thought that the flow path in the northern hot-spring area is determined by the fractures in the volcanic rocks. Fracture zones have been created by past fault activity, enabling hot-spring water to flow from the deeper side of the volcanic rocks.

## 6. Conclusion

This study presents an analysis of the gravity data over the Beppu geothermal field. The results of using edge-detecting filters on the gravity data indicate that high HD and INH areas exist in the western and southern parts of the study area. These high HD and INH areas correspond to the Asamigawa Fault in the southern part of the study area, but deviate 1 km east of the Kankaiji hot spring to the north. The hot-spring area in the southern part of the study area, near Horita, Kankaiji, and Hamawaki, corresponds to these high-value areas. The distribution of the depths of the 3-D gravity basement enable delineation of the interface between the volcanic basement rocks and the fan deposits. As previously mentioned, the results of the gravity analysis indicate that the flow-path structure differs between the northern and southern parts of the hot-spring area. Fracture zones have been created by past fault activity, enabling hot-spring water to flow from the deeper side of the volcanic rocks. This study provides an understanding of the underground structure of the Beppu hydrothermal systems. To fully understand the long-term sustainability of the hot springs, further geothermal modeling and numerical simulation of hydrothermal systems should be conducted.

## References

- Abdelzaher, M., Nishijima, J., El-Qady, G., Aboud, E., Masoud, O., Soliman, M., Ehara, S., 2011. Gravity and magnetotelluric investigations to elicit the origin of Hammam Faraon hot spring, Sinai Peninsula, Egypt. *ACTA Geophys.* 59, 633–656. <http://dx.doi.org/10.2478/s11600-011-0006-4>.
- Allis, R.G., Yusa, Y., 1989. Fluid flow processes in the Beppu geothermal system, Japan. *Geothermics* 18, 743–759. [http://dx.doi.org/10.1016/0375-6505\(89\)90104-1](http://dx.doi.org/10.1016/0375-6505(89)90104-1).
- Chida, N., Ikeda, Y., Nakada, T., Okada, A., Une, H., 2000. 1:25000 Active Fault Map in Urban Area, Beppu. Geographical Survey Institute of Japan (in Japanese).
- Cooper, G.R.J., Cowan, D.R., 2006. Enhancing potential field data using filters based on the local phase. *Comput. Geosci.* 32, 1585–1591. <http://dx.doi.org/10.1016/j.cageo.2006.02.016>.

Please cite this article in press as: Nishijima, J., Naritomi, K., Interpretation of gravity data to delineate underground structure in the Beppu geothermal field, central Kyushu, Japan. *J. Hydrol.: Reg. Stud.* (2015), <http://dx.doi.org/10.1016/j.ejrh.2015.11.022>

- Cordell, L., Henderson, R.G., 1968. Iterative three-dimensional solution of gravity anomaly data using a digital computer. *Geophysics* 33, 596–601.
- Cordell, L., Grauch, V.J.S., 1985. Mapping basement magnetization zones from aeromagnetic data in the San Juan Basin, New Mexico. In: Hinz, W.J. (Ed.), *The Utility of Regional Gravity and Magnetic Anomaly Maps*. Society for the Exploration of Geophysics, pp. 181–197.
- Geological Survey of Japan, AIST, 2013. Gravity Database of Japan, DVD Edition. Geological Survey of Japan, National Institute of Advanced Industrial Science and Technology.
- Geological Survey of Japan, AIST, 2014. Seamless Digital Geological Map of Japan 1: 200,000. Jan 14, 2014 Version. Geological Survey of Japan, National Institute of Advanced Industrial Science and Technology.
- Hoshizumi, H., Ono, K., Mimura, K., Noda, T., 1988. Geology of the Beppu district With geological sheet map of 1:50,000. *Geol. Surv. Japan*, 131 (in Japanese with English abstract).
- Itoh, Y., Kusumoto, S., Takemura, K., 2014. Evolutionary process of Beppu Bay in central Kyushu, Japan: A quantitative study of the basin-forming process controlled by plate convergence modes. *Earth Planets Space* 66, 74, <http://dx.doi.org/10.1186/1880-5981-66-74>.
- Kamata, H., 1989. Volcanic and structural history of the Hoho volcanic zone, central Kyushu, Japan. *Bull. Volcanol.* 51, 315–332, <http://dx.doi.org/10.1007/bf01056894>.
- Kusumoto, S., Fukuda, Y., Takemoto, S., Yusa, Y., 1996. Three-dimensional subsurface structure in the eastern part of the Beppu-Shimabara Graben Kyushu, Japan, as revealed by gravimetric data. *J. Geod. Soc. Japan* 42, 167–181, <http://dx.doi.org/10.11366/sokuchi1954.42.167>.
- Li, L., Huang, D., Han, L., Ma, G., 2014. Optimised edge detection filters in the interpretation of potential field data. *Explor. Geophys.* 45, 171–176, <http://dx.doi.org/10.1071/eg13059>.
- Murata, Y., 1993. Estimation of optimum average surficial density from gravity data: An objective Bayesian Approach. *J. Geophys. Res.* 98, 12097, <http://dx.doi.org/10.1029/93jb00192>.
- New Energy Development Organization, 1990. Regional exploration of geothermal fluid circulation system, Tsurumidake area. National Geothermal Resources Exploration Project (3rd Phase), p. 88 (in Japanese).
- Okabe, M., 1979. Analytical expressions for gravity anomalies due to homogeneous polyhedral bodies and translations into magnetic anomalies. *Geophysics* 44, 730–741.
- Ohsawa, S., Yusa, Y., Kitaoka, K., 1994. Flow paths of thermal groundwaters in the southern part of Beppu, Japan. *J. Hot Spring Sci. Japan* 44, 199–208 (in Japanese with English abstract).
- Ohsawa, S., Yusa, Y., 1996. Flow paths of thermal ground water inferred from the chemical composition of hot spring water in the northern part of Beppu, Japan, in: Report of a Study on Geothermal Fluid Flow Processes and Subsurface Structure. pp. 103–114 (in Japanese).
- Rao, P.R., Swamy, K.V., Radhakrishna Murthy, I.V., 1999. Inversion of gravity anomalies of three-dimensional density interfaces. *Comput. Geosci.* 25, 887–896.
- Represas, P., Monteiro Santos, F.A., Ribeiro, J., Ribeiro, J.A., Almeida, E.P., Gonçalves, R., Moreira, M., Mendes-Victor, L.A., 2013. Interpretation of gravity data to delineate structural features connected to low-temperature geothermal resources at Northeastern Portugal. *J. Appl. Geophys.* 92, 30–38, <http://dx.doi.org/10.1016/j.jappgeo.2013.02.011>.
- Sasada, M., 1984. Basement structure of the Hoho geothermal area, central Kyushu, Japan. *J. Japan Geotherm. Energy Assoc.* 21, 1–11 (in Japanese with English abstract).
- Sasada, M., 1987. Pre-tertiary basement rocks of Hoho area, central Kyushu, Japan. *Bull. Geol. Surv. Japan* 38, 385–422 (in Japanese with English abstract).
- Smith, W.H.F., Wessel, P., 1990. Gridding with continuous curvature splines in tension. *Geophysics* 55, 293–305.
- Tada, T., 1984. Spreading of the Okinawa Trough and its relation to the crustal deformation in Kyushu. *J. Seismological Soc. Japan*. 2nd ser. 37, 407–415 (in Japanese with English abstract).
- Yusa, Y., Ohsawa, S., Kitaoka, K., 2000. Long-term changes associated with exploitation of the Beppu hydrothermal system, Japan. *Geothermics* 29, 609–625, [http://dx.doi.org/10.1016/s0375-6505\(00\)00025-0](http://dx.doi.org/10.1016/s0375-6505(00)00025-0).